Geophysical Research Letters

RESEARCH LETTER
10.1029/2022GL100355

Key Points:

- Physics-based simulations reveal relationships between delta morphology and the balance of river, wave, and tidal sediment fluxes
- Rivers create channels and tides roughen the shoreline, whereas waves smooth the shoreline, decrease channel number, and can create spits
- The simulations are consistent with the morphology of field deltas and confirm the 50-year-old hypothesis of Galloway (1975, https://archives.datapages.com/data/hgssp/data/022/022001/87_hgs0220087.htm)

Supporting Information:

Supporting Information may be found in the online version of this article.

Correspondence to:

C. M. Broaddus,
cbroaddu@uci.edu

Citation:

Broaddus, C. M., Vulis, L. M., Nienhuis, J. H., Tejedor, A., Brown, J., Foufoula-Georgiou, E., & Edmonds, D. A. (2022). First-order river delta morphology is explained by the sediment flux balance from rivers, waves, and tides. *Geophysical Research Letters*, *49*, e2022GL100355. https://doi.org/10.1029/2022GL100355

Received 8 JUL 2022
Accepted 1 NOV 2022

Author Contributions:

Conceptualization: C. M. Broaddus, L. M. Vulis, J. H. Nienhuis, A. Tejedor, J. Brown, E. Foufoula-Georgiou, D. A. Edmonds
Data curation: C. M. Broaddus
Formal analysis: C. M. Broaddus, L. M. Vulis, J. H. Nienhuis, A. Tejedor, J. Brown, E. Foufoula-Georgiou, D. A. Edmonds
Funding acquisition: E. Foufoula-Georgiou, D. A. Edmonds
Investigation: C. M. Broaddus
Methodology: C. M. Broaddus, L. M. Vulis, J. H. Nienhuis, A. Tejedor, J. Brown, E. Foufoula-Georgiou, D. A. Edmonds

First-Order River Delta Morphology Is Explained by the Sediment Flux Balance From Rivers, Waves, and Tides

C. M. Broaddus[1,2], L. M. Vulis[2], J. H. Nienhuis[3], A. Tejedor[2,4], J. Brown[1], E. Foufoula-Georgiou[2,5], and D. A. Edmonds[1]

[1]Department of Earth and Atmospheric Sciences, Indiana University, Bloomington, IN, USA, [2]Department of Civil and Environmental Engineering, University of California, Irvine, Irvine, CA, USA, [3]Department of Physical Geography, Utrecht University, Utrecht, The Netherlands, [4]Department of Science and Engineering, Sorbonne University, Abu Dhabi, UAE, [5]Department of Earth System Science, University of California, Irvine, CA, USA

Abstract We present a novel quantitative test of a 50-year-old hypothesis which asserts that river delta morphology is determined by the balance between river and marine influence. We define three metrics to capture the first-order morphology of deltas (shoreline roughness, number of distributary channel mouths, and presence/absence of spits), and use a recently developed sediment flux framework to quantify the river-marine influence. Through analysis of simulated and field deltas we quantitatively demonstrate the relationship between sediment flux balance and delta morphology and show that the flux balance accounts for at least 35% of the variance in the number of distributary channel mouths and 42% of the variance in the shoreline roughness for real-world and simulated deltas. We identify a tipping point in the flux balance where wave influence halts distributary channel formation and show how this explains morphological transitions in real world deltas.

Plain Language Summary River deltas are ecologically and economically important, and each delta is unique in terms of its environmental conditions and overall form. We test a 50-year-old hypothesis that qualitatively relates the overall form of a delta (in terms of its shoreline and channel network) to the balance between river and marine influence. We develop a suite of simulated river deltas using a physics-based numerical model. We quantitatively describe the overall form for each of the simulated deltas and for a globally-distributed set of real-world deltas. The simulations and global deltas indeed exhibit relationships between their overall form and the balance of river and marine influence. Deltas with little to no marine influence have abundant channel mouths and rough shorelines. Tides act to roughen the shoreline but do not affect the number of distributary channel mouths. Waves tend to smooth the shoreline and reduce the number of distributary channel mouths. Waves may also lead to the formation of barrier islands and sand spits, though these features do not necessarily indicate wave "dominance." These results confirm the hypothesis from the 1970's while adding important information about the morphological transitions between different end-member "type" deltas.

1. Introduction

The morphologies of global river deltas are characterized to a first-order by their channel networks, shorelines, and planform geometries (Galloway, 1975). These characteristics can vary significantly between deltas and can impact their resilience (Hoitink et al., 2020; Tejedor et al., 2015; Tessler et al., 2015), population capacity (Edmonds et al., 2020), and stratigraphy (Galloway, 1975; Wright & Coleman, 1973). Elucidating the controls on river delta morphology is critical for future management and mitigation strategies, especially in light of rising sea levels and coastal subsidence (Nicholls et al., 2021; Shirzaei et al., 2020), increased storm frequency and intensity, and river catchment modification by humans. Despite this need, a quantitative understanding of what sets first-order delta morphology is lacking.

In the prevailing hypothesis of Galloway (1975), delta morphology is set by the balance of fluvial, wave, and tidal energy fluxes. The intuitive nature of this theory has made it the standard for delta classification, yet the axes of the ternary diagram that define it are qualitative, limiting its predictive capacity and inhibiting a quantitative test of the theory. More recent field (Nienhuis et al., 2015; Passalacqua et al., 2013; Syvitski & Saito, 2007) experimental (Finotello et al., 2019; Ganti et al., 2016; Hoyal & Sheets, 2009) and numerical (Ashton & Giosan, 2011;

Project Administration: E. Foufoula-Georgiou, D. A. Edmonds
Resources: C. M. Broaddus, L. M. Vulis, J. H. Nienhuis, D. A. Edmonds
Software: C. M. Broaddus, J. H. Nienhuis, J. Brown, D. A. Edmonds
Supervision: D. A. Edmonds
Validation: C. M. Broaddus
Visualization: C. M. Broaddus
Writing – original draft: C. M. Broaddus, D. A. Edmonds
Writing – review & editing: C. M. Broaddus, L. M. Vulis, J. H. Nienhuis, A. Tejedor, J. Brown, E. Foufoula-Georgiou, D. A. Edmonds

Canestrelli et al., 2014; Edmonds & Slingerland, 2010; Geleynse et al., 2011; Leonardi et al., 2013; Rossi et al., 2016) work has clarified how river, wave, or tide-dominated end-members grow and even created predictive relationships for certain morphologic features based on the balance of two fluxes. However, it is unclear if these predictions hold for deltas under the combined influence of all three fluxes.

Recent work (Nienhuis et al., 2015, 2018, 2020) has quantified the axes of Galloway's ternary diagram by formulating relationships for the river, wave, and tidal sediment fluxes experienced by the delta. Here we use this newly quantified framework to test the link between delta morphology and flux balance.

2. Materials and Methods

2.1. Ensemble of Simulated Deltas

While several physically-based or reduced complexity models for numerically simulating river deltas exist (Caldwell & Edmonds, 2014; Edmonds & Slingerland, 2007; Geleynse et al., 2011; Lauzon et al., 2019; Liang et al., 2015; Rossi et al., 2016; Seybold et al., 2007), there have been few, if any, successful attempts at reproducing the diversity of delta morphology under the combined influence of rivers, waves, and tides. Most efforts have focused on end-member morphology (Geleynse et al., 2011) or morphological variability in response to a single flux (Rossi et al., 2016; Seybold et al., 2007). Using Delft3D (Lesser et al., 2004), we simulate 62 river deltas with non-cohesive sediment (grain size = 135 μm) that span the ternary space by varying the magnitude of wave and tidal forcings while holding river discharge and factors not explicitly included in the sediment flux framework (such as sediment characteristics) constant. Simulations represent delta evolution on timescales ranging from decades to centuries depending on assumptions regarding the frequency-magnitude relationships of large floods and wave events (see Text S1 and Figure S1 in Supporting Information S1 for model setup details).

Simulations are placed in the ternary space according to the balance of their fluvial, wave, and tidal fluxes (Q_{river}, Q_{wave}, Q_{tide}, respectively) (Figure S2a in Supporting Information S1). Ratios of these fluxes describe the relative contribution of one flux or another (Equation 1).

$$r_x = \frac{Q_x}{Q_{river} + Q_{wave} + Q_{tide}} \quad (1)$$

Q_{river} is taken as the time averaged flux entering the basin prior to delta inception, measured near the upstream boundary. We estimate the values of Q_{wave} following the methodology of Nienhuis et al. (2015) which uses the CERC equation to estimate a maximum potential littoral transport for each delta. We estimate Q_{tide} following Nienhuis et al. (2018) (which estimates Q_{tide} according to the tidal prism), diverging only in our definition of slope, which we estimate assuming an equilibrium normal flow profile for distributaries. The estimated slope for all runs is roughly 10^{-4}, which matches the slope of our feeder channel. Our simulation ensemble covers a large portion of the ternary space with a focus on intermediate flux balances (Figure S1, Table S1 in Supporting Information S1).

2.2. Morphological Metrics

We quantify the morphology of simulated deltas using three simple metrics that characterize the shoreline and distributary channel network (Figure 1).

Shorelines are defined from binary wet/dry maps for every model output timestep using the opening angle method of Shaw et al. (2008), which addresses the problem of shoreline ambiguity across river mouths. This method defines for every wet cell the angle that spans the view into open water (a flat shoreline has a 180-degree view). The shoreline is defined by selecting a given "opening angle"; smaller angles produce shorelines that precisely follow the land-water interface, while larger angles smooth over indentations.

We define shoreline roughness (ρ^*) for each delta by comparing the lengths of the shorelines obtained using opening angles of 45 (L_{45}) and 120° (L_{120}) (2). This definition is less biased to delta-scale shoreline concavities than similar shoreline roughness metrics that use the length of a convex hull as the normalizing length (Geleynse et al., 2012). ρ^* is thus focused on roughness at sub-delta scales.

$$\rho^* = \frac{L_{45}}{L_{120}} \quad (2)$$

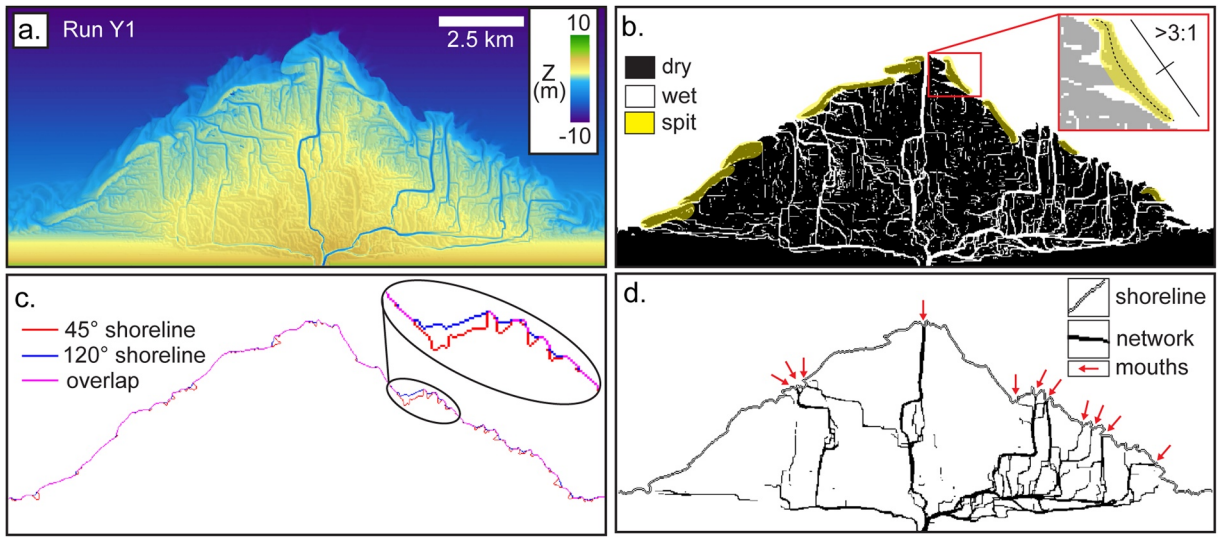

Figure 1. Example of a simulated delta and schematics illustrating morphological metrics. All panels show the final output of a run with approximately equal river, wave, and tidal sediment fluxes (Run Y1, see Supporting Information S1). (a) Shows the topobathymetry as elevation relative to sea level, (b) shows a binary inundation map highlighting the presence of spits, (c) illustrates the various shorelines used to compute the shoreline roughness, and (d) shows the intersections of the distributary channel network and shoreline that define channel mouths.

Channel networks are defined as areas upstream of the shoreline where flow depth is greater than 10 cm, velocity is greater than 0.01 m/s (following Caldwell and Edmonds (2014)), and sediment transport is at least 1% of the sediment transport at the delta apex. These threshold values were chosen to provide a complete representation of the significant (in terms of water and sediment transport) portions of the channel network. Changing the threshold values by a factor of 2 in either direction leads to small differences in the details of the networks but does not affect the total number of distributary channel mouths.

We define distributary channel mouths as locations where the channel network and the shoreline intersect. To avoid over-counting for channels that intersect the shoreline at low angles, we apply a 1 pixel buffer to each "mouth" pixel that groups nearby pixels into one connected component. This method could result in distinct distributaries at the shoreline being unintentionally grouped into one channel mouth; our count for the number of distributary channel mouths (N_{ch}) is likely a slight underestimate. N_{ch} and ρ^* are averaged from low tide timesteps over the final 1/3 of the simulation.

The presence or absence of spits (S_{PA}) is determined by visual inspection of binary inundation maps. We define spits as shore-parallel, elongated (greater than 3:1 aspect ratio) dry areas at or near the delta shoreline. Where S_{PA} is uncertain, we err on the side of absence. Because of the highly transient nature of spits and barrier islands, S_{PA} is determined based on the final low-tide output for each model run.

2.3. Statistics

We assess statistically significant differences in the morphological metrics across the ternary space categorically according to the dominant flux (where each delta plots in Figure S2b in Supporting Information S1). We use a threshold p-value of 0.05 to determine significance for all statistical tests. We use logistic regression to compare the probability of spit occurrence between river, wave, and tide-influenced categories. For ρ^* and N_{ch}, we use the Kruskal-Wallis H-test to compare the mean ranks of simulations in river, wave, and tide-influenced categories. In cases where the categorical tests show significant differences (N_{ch} and ρ^* for simulations and field deltas) we perform multiple comparison tests to determine which categories were distinct from each other.

To assess relationships between the morphological metrics and wave or tide-dominance (r_{wave} or r_{tide}), we employ weighted least squares linear regression (N_{ch} and ρ^* metrics for field deltas) and logistic regression (S_{PA}). For the linear regressions, we use iteratively weighted least squares to address heteroscedasticity in N_{ch} and ρ^*, and log-transform r_{wave} and r_{tide} values for all regressions to increase normality in the sample distribution. We assess

goodness of fit for the linear regressions using R^2. For the logistic regressions, we assess goodness of fit using the Chi-square test.

To summarize the proportion of metric variability explained by the balance of all three fluxes (and to ensure our results and interpretations are robust across different statistical assessments) we perform multiple linear regression of the relative influence values (predictor variables) against the metric values (response variable). A separate regression is performed for each metric (N_{ch} and ρ^*), and the regressions are performed separately for simulations and field deltas. We assess goodness of fit using R^2.

3. Results and Discussion

3.1. Qualitative Assessment

Our simulations recreate much of the morphological diversity observed in real-world delta systems (Figure 2). End-member simulations show morphological characteristics that are hallmarks of these delta types. In river-dominated simulations (those lacking substantial marine influence), the deltas develop complex distributary channel networks with an abundance of bifurcations and river mouths. Shorelines are lobate with semicircular to irregular geometries (Figures 2a and 2d). This morphology is the result of progradation via mouth-bar induced bifurcation and avulsion of distributaries and is common for deltas with low basin energy (relative to fluvial sediment flux) and non-cohesive sediment loads (Edmonds & Slingerland, 2010), such as the Volga Delta (Figure 2a).

Tide-dominated simulations exhibit rough shorelines (relative to river or wave-dominated delta shorelines when observed at the same scale), large subaqueous platforms, and headless channels that are disconnected from the distributary network (Figure 2e). Headless channels are ubiquitous on tide-dominated deltas in the field and are self-formed or relict abandoned distributaries maintained via bi-directional tidal flow and landward-decreasing shear stresses (Fagherazzi, 2008; Hood, 2010). These deltas also have large subaqueous platforms that extend seaward from the shoreline, consistent with field deltas subjected to significant tidal influence (Goodbred & Saito, 2012; Rossi et al., 2016). Rough shorelines are common features of tide-dominated deltas in the field such as the Orinoco delta (Figure 2b) (Galloway, 1975; Geleynse et al., 2011; Rossi et al., 2016), and in our simulations roughness results from a combination of headless tidal channels and distributary channels perturbing the shoreline as protrusions and indentations. This effect may be exacerbated by ebb-induced mouth bar erosion and elongation of distributary channels (Geleynse et al., 2011; Leonardi et al., 2013; Rossi et al., 2016).

Wave-dominated simulations exhibit relatively simple distributary channel networks with a limited number of channel mouths (Figure 2f). This observation is consistent with the hypothesis that high wave energy inhibits mouth bar formation and resultant bifurcation-induced distributary network development (Jerolmack & Swenson, 2007; Nardin & Fagherazzi, 2012). Wave-dominated simulations are also characterized by sand spits and barrier islands that form near distributary mouths and may eventually amalgamate to the shoreline and form beach ridges (Figure 2f). These features are indicators of wave-induced alongshore sediment transport and are thought to be diagnostic of wave-influence on delta morphology in field deltas (Ashton & Giosan, 2011; Galloway, 1975; Nienhuis et al., 2013; Syvitski & Saito, 2007; Wright & Coleman, 1973). Wave-dominated simulations are generally semicircular to cuspate in planform, with relatively smooth shorelines (Figure 2f). These characteristics resemble field deltas (such as the Mahanadi delta, Figure 2c) and are thought to be the result of waves acting to diffuse the shoreline through erosion (Ashton & Giosan, 2011; Jerolmack & Swenson, 2007; Nardin & Fagherazzi, 2012; Nienhuis et al., 2013).

The end-member morphological characteristics are present to varying degrees in deltas with intermediate flux balances and combine to create a spectrum of possible morphologies (Figure S3 in Supporting Information S1). To assess variation in the end-member characteristics across flux balance parameter space, we apply N_{ch}, ρ^*, and S_{PA} to quantitatively describe these different aspects of delta morphology.

3.2. Quantifying the Influence of Flux Balance on the Morphology of Simulated Deltas

There are statistically significant differences in ρ^* between the three groups: tide-influenced deltas have the highest ρ^*, wave-influenced have the lowest, and river-influenced are intermediate (Figure 3a and Table S2 in Supporting Information S1). ρ^* increases with r_{tide} and decreases with r_{wave} across the range of simulated flux

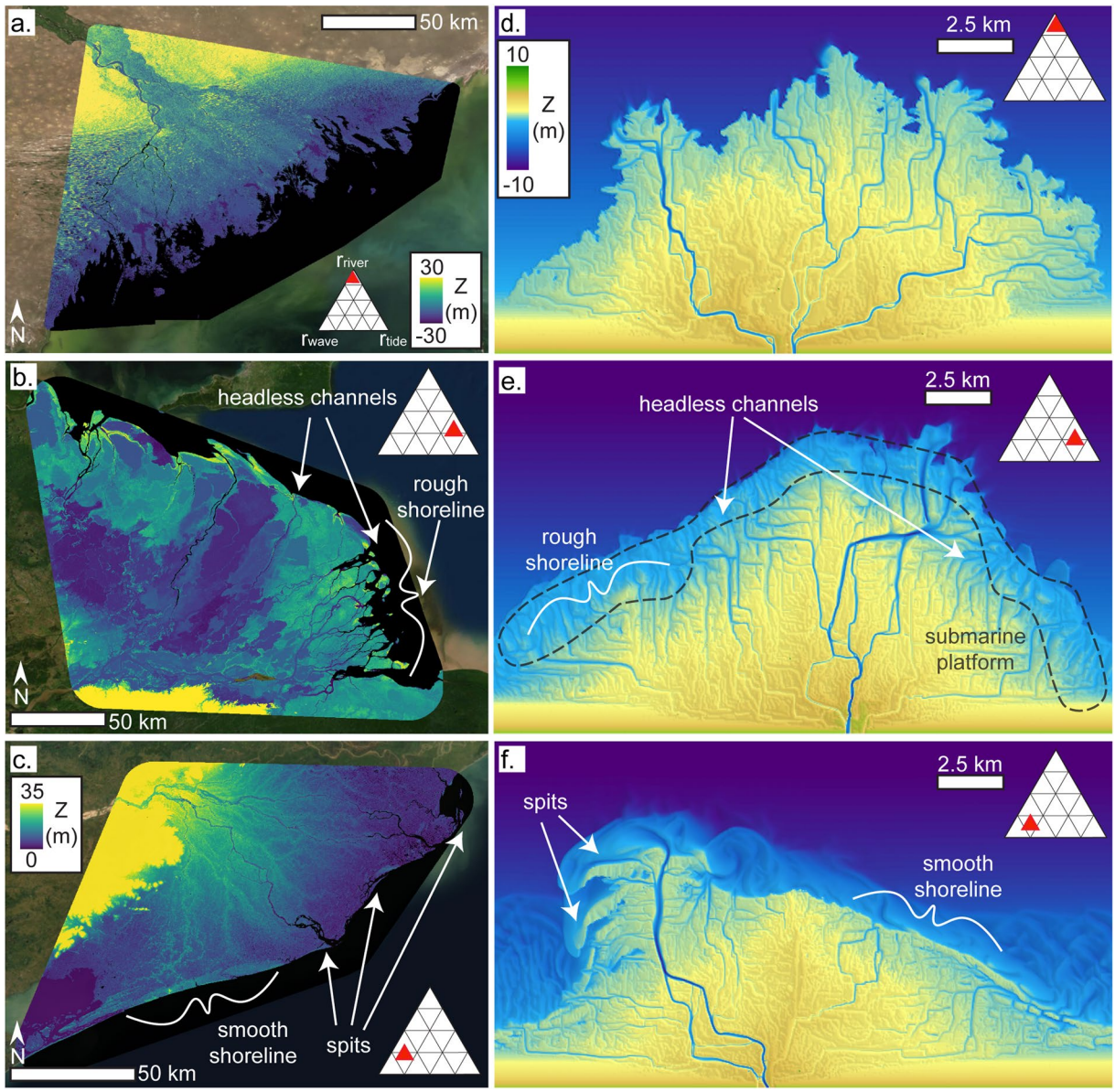

Figure 2. Examples of near end-member deltas from field and simulated datasets, with arrows and labels denoting characteristic features of wave and tide-dominated end members. Field delta topography is displayed in meters above sea-level, sourced from 1 arc second SRTM data (Farr & Kobrick, 2000). Simulation topobathymetry displayed in meters relative to sea level. (a) River-dominated Volga delta, Russia. (b) Tide-dominated Orinoco delta, Venezuela. (c) Wave-dominated Mahanadi delta, India. (d) River-dominated simulation, Run O1. (e) Tide-dominated simulation, Run L2. (f) Wave-dominated simulation, Run U2.

balances (Figures 4a and 4d). This occurs because the processes acting to roughen the shoreline–headless channel formation, ebb-enhanced distributary elongation and resultant shoreline perturbation–increase gradually with tidal sediment flux (Finotello et al., 2019; Leonardi et al., 2013). By contrast, processes acting to smooth the shoreline–erosion and deposition due to gradients in longshore transport–increase gradually with the wave-driven sediment flux (Ashton & Giosan, 2011; Nienhuis et al., 2013).

There are statistically significant differences in the mean N_{ch} between wave-influenced, and river or tide-influenced simulations where river and tide-influenced deltas have greater N_{ch} than wave-influenced deltas (Figure 3b, Table S2 in Supporting Information S1). For deltas with $r_{wave} < 0.1$ there is significant variability and no clear trend in N_{ch} likely reflecting a range of processes that contribute to channel formation (Figures 4b and 4e). Waves decrease N_{ch}, consistent with theory (Jerolmack & Swenson, 2007; Nardin & Fagherazzi, 2012; Wright & Coleman, 1973), but only when $r_{wave} > 0.1$. Interestingly, an order of magnitude increase in r_{wave} from 0.1 to 1 leads to a drastic

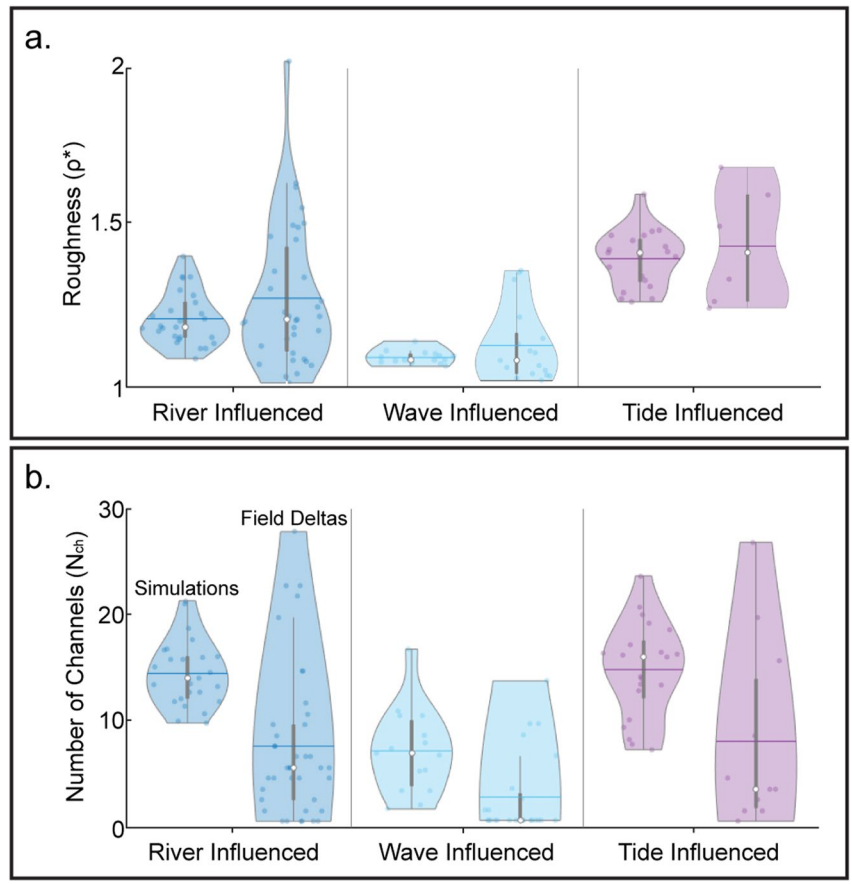

Figure 3. Morphological differences between river, wave, and tide-influenced deltas. Categorical distributions of (a) ρ^* and (b) N_{ch} metrics shown as violin plots. Note the clear separation between the ρ^* of wave and tide-influenced deltas in (a), and the low values of N_{ch} for wave-influenced deltas in (b).

reduction in N_{ch}, at times producing deltas with a single distributary channel mouth. Our simulations showed no significant relationship between r_{tide} and N_{ch}.

We used logistic regression to categorically assess the relationship between a delta's most influential flux and S_{PA}. We found no statistical significance, indicating that the most influential flux is a poor predictor of S_{PA}. However, logistic regression of r_{wave} against S_{PA} shows a statistically significant relationship, confirming the role of waves in determining spit occurrence (Figure 4c). These seemingly contradictory results occur because spits are present throughout most of ternary space (including many of the "river-influenced" simulations) but are absent when $r_{wave} < 0.25$ (Figure 4f). Spit development does not appear to be influenced by tides as there is no significant relationship between r_{tide} and S_{PA}.

3.3. Comparison With Field Deltas

Isolating the influence of flux balance on morphology is challenging for real-world deltas because other controls such as vegetation (Lauzon & Murray, 2018; Nardin et al., 2016), basin geometry (Geleynse et al., 2011) and sediment properties (Caldwell & Edmonds, 2014) can also affect shoreline and channel network development. Still, if Galloway's hypothesis is correct then deltas in the field should bear the influence of their flux balance to a first order. We compare our simulations with a set of globally-distributed river deltas chosen from existing datasets (Caldwell et al., 2019; Syvitski & Saito, 2007) with the goal of sampling the variety of flux balances observed in nature (Figure S2d and Table S3 in Supporting Information S1). For the field deltas, ρ^* is calculated following the same methodology as the simulations, N_{ch} is determined from the method of Syvitski and Saito (2007), and S_{PA} is determined from Landsat imagery and water occurrence maps (Pekel et al., 2016), using the same definition

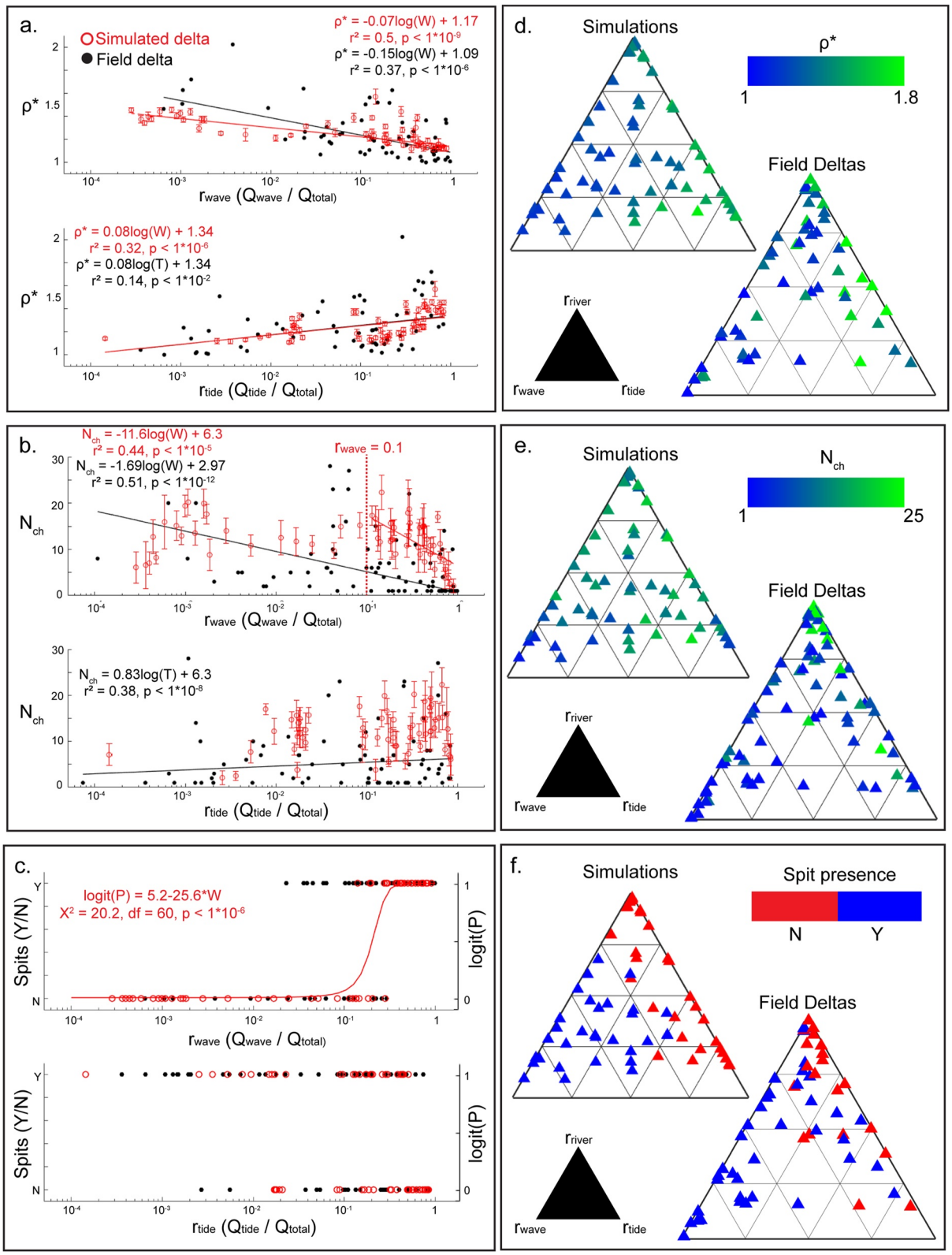

Figure 4. Morphometric trends for simulated and field deltas. (a) ρ^* decreases with r_{wave} and increases with r_{tide} (b) N_{ch} decreases with r_{wave}, with simulations showing a rapid decrease in N_{ch} for $r_{wave} > 0.1$. (Field deltas with greater than 30 channels are not shown here for the sake of visualization, see Figure S5 in Supporting Information S1). (c) S_{PA} appears to be related to wave influence, but field deltas indicate it is not diagnostic of wave dominance. (d) ρ^* plotted in ternary space, decreasing with r_{wave} and increasing with r_{tide}. (e) N_{ch} plotted in ternary space, decreasing with r_{wave}. (f) S_{PA} plotted in ternary space, showing ubiquitous occurrence of spits on wave-dominated deltas. Error bars in (a and b) reflect the standard deviation in the metric value over the final 1/3 of the run duration.

as for our simulations. Transport ratios for field deltas are based on sediment flux values reported by Nienhuis et al. (2020) (see Text S3 in Supporting Information S1 for detail).

Categorical binning of the data shows that river, wave, and tide-influenced field deltas have significantly different ρ^* and N_{ch} (Figure 3 and Table S1 in Supporting Information S1), in agreement with our simulations. The observed trends (with respect to r_{wave} and r_{tide}) also follow the model predictions; ρ^* increases with r_{tide} and decreases with r_{wave} (Figures 4a and 4d), whereas N_{ch} decreases with increasing r_{wave} (Figures 4b and 4e). That said, the scatter in the N_{ch} field data is substantial, likely reflecting other important variables. Interestingly, we find a significant relationship between N_{ch} and r_{tide} for field deltas that is not observed in our simulations (Figure 4b). Finally, as with the simulations there are no significant differences in S_{PA} among river, wave, and tide-influenced deltas. While S_{PA} is related to r_{wave} (Figure 4f), the most influential flux is not a good predictor for spit presence/absence.

4. Discussion and Conclusions

Our results confirm the 50-year-old hypothesis of Galloway (1975) (with some important deviations) and quantitatively demonstrate the relationship between delta morphology and the relative flux contributions from rivers, waves, and tides. River-influenced deltas have a relatively high number of distributary channel mouths (N_{ch}), average shoreline roughness (ρ^*), and may or may not have spits. Tide-influenced deltas are distinguished by their rough shorelines ($\rho^* \approx 1.4$), while wave-influenced deltas are distinguished by their smooth shorelines ($\rho^* \approx 1.1$), smaller number of distributary channels (on average less than half as many as river and tide-influenced deltas) and the common occurrence of spits and barrier islands.

Multiple regression shows that the relative influence values (r_{river}, r_{wave}, r_{tide}) explain 42% of the variance in ρ^* and 35% of the variance in N_{ch} for the field deltas (Table S4 in Supporting Information S1). These values are even higher for the simulations (62% for ρ^* and 36% for N_{ch}). We note that the variance explained by these fits, as well as those of all other linear regression models reported here, represent lower bounds for the morphological variability explained by the flux balance. It is possible that higher-order fits could explain greater proportions of the variability given the same inputs. Still, our analyses show that at least one-third of the variability in ρ^* and N_{ch} is explained by the monotonic relationships hypothesized by Galloway (1975) and other authors.

Mapping these characteristics in ternary space illuminates important nuances in the relationships between flux balance and morphology. For example, spits and barrier islands were cited by Galloway (1975) as being diagnostic of wave-dominance in deltaic systems. However, our simulations and field delta analysis show that they are present throughout most of ternary space and thus are not a good indicator of flux balance. A better indicator for wave-dominance is the number of distributary channel mouths, which is relatively agnostic to flux balance except in strongly wave-influenced deltas (i.e., N_{ch} decreases with r_{wave} when $r_{wave} > 0.1$). These relationships have important implications for interpreting ancient deltaic systems, for managing modern deltas, and for predicting how delta morphology might change in response to shifts in the flux balance.

Human activity has led to changes in fluvial sediment loads at many river mouths, which alters the flux balance of those deltas and shifts their positions on the ternary diagram. On the Ebro, Po, and Rhone river deltas, anthropogenically-driven decreases in Q_{river} of up to 90% over the past millennium (Maselli & Trincardi, 2013) led to substantial decreases in the number of distributary channels (Mikhailova, 2003). Each of these systems were historically positioned near the $r_{wave} = 0.1$ "tipping point" identified in our simulations (Figure 4b); the large reductions in Q_{river} pushed r_{wave} past the tipping point and caused the decreases in N_{ch}. Other shifts toward wave-influenced morphology (such as shoreline smoothing) have coincided with anthropogenic flux decreases in these and other systems (Mikhailova, 2003). We consider these as examples of morphological shifts in response to changing flux balances.

We note that the framework presented here is not intended to directly predict the morphological metric values given the input forcing values. Metric values vary temporally even for a delta with constant forcing due to autogenic processes, and depend partially on the scale of measurement. There is also significant uncertainty in the sediment flux values of natural delta systems due to the difficulty of measuring these quantities (see Text S2 in Supporting Information S1). These uncertainties, when combined with the large number of other factors affecting morphology, make a truly predictive relationship elusive. Rather, our goal is to quantitatively test the

morphological trends hypothesized by Galloway, and to gain insight into the nature of how morphology varies across the flux balance parameter space.

Our controlled simulations suggest that the flux balance sets the first-order morphology of the delta, and these results generally agree with the field deltas, though there are some differences. These differences highlight the importance of other factors in predicting delta morphology. Median grain size and cohesion of fluvial sediment have been shown to strongly influence delta morphology (Caldwell & Edmonds, 2014), particularly in systems with low wave energy, and may lead to different morphologies than identified here. Quantitatively incorporating sediment characteristics into the flux balance framework (by analogy with Orton and Reading (1993)) is non-trivial but could increase predictability of the morphometrics described here. It would also be beneficial to use this framework to test how vegetation, river-ice, or permafrost-affected soil modify the channel networks and planform delta morphology (Lauzon & Murray, 2018; Lauzon et al., 2019; Nardin et al., 2016; Passalacqua et al., 2013). Further complicating matters is the ubiquitous seasonality of each of the fluxes, coupled with the observation that most geomorphic work occurs during brief periods of high energy and that geomorphic response often depends on the sequence of events rather than just their magnitudes (Kwang & Parker, 2019). Moving toward a fully predictive framework for river delta morphology will require reconciling these complex interactions and other controlling factors with the flux balance paradigm.

Data Availability Statement

Global Surface Water images used for field delta analyses and Delft3D simulation outputs (including sensitivity tests) for the analyzed timesteps are available at https://doi.org/10.5281/zenodo.6804246. Code required to perform the analysis and create figures are available at https://doi.org/10.5281/zenodo.6804246. Supporting information available at https://doi.org/10.5281/zenodo.6804246.

Acknowledgments
This research was supported by NSF Earth Sciences Grant 1812019 (awarded to D.A. Edmonds) and 1811909 (awarded to E. Foufoula Georgiou).

References

Ashton, A. D., & Giosan, L. (2011). Wave-angle control of delta evolution. *Geophysical Research Letters*, *38*(13), L13405. https://doi.org/10.1029/2011GL047630

Caldwell, R. L., & Edmonds, D. A. (2014). The effects of sediment properties on deltaic processes and morphologies: A numerical modeling study. *Journal of Geophysical Research: Earth Surface*, *119*(5), 961–982. https://doi.org/10.1002/2013JF002965

Caldwell, R. L., Edmonds, D. A., Baumgardner, S., Paola, C., Roy, S., & Nienhuis, J. H. (2019). A global delta dataset and the environmental variables that predict delta formation on marine coastlines. *Earth Surface Dynamics*, *7*(3), 773–787. https://doi.org/10.5194/esurf-7-773-2019

Canestrelli, A., Lanzoni, S., & Fagherazzi, S. (2014). One-dimensional numerical modeling of the long-term morphodynamic evolution of a tidally-dominated estuary: The Lower Fly River (Papua New Guinea). *Sedimentary Geology*, *301*, 107–119. https://doi.org/10.1016/j.sedgeo.2013.06.009

Edmonds, D. A., & Slingerland, R. L. (2007). Mechanics of river mouth bar formation: Implications for the morphodynamics of delta distributary networks. *Journal of Geophysical Research*, *112*(F2), F02034. https://doi.org/10.1029/2006JF000574

Edmonds, D. A., & Slingerland, R. L. (2010). Significant effect of sediment cohesion on delta morphology. *Nature Geoscience*, *3*(2), 105–109. https://doi.org/10.1038/ngeo730

Edmonds, D. A., Caldwell, R. L., Brondizio, E. S., & Siani, S. M. O. (2020). Coastal flooding will disproportionately impact people on river deltas. *Nature Communications*, *11*(1), 4741. https://doi.org/10.1038/s41467-020-18531-4

Fagherazzi, S. (2008). Self-organization of tidal deltas. *Proceedings of the National Academy of Sciences*, *105*(48), 18692–18695. https://doi.org/10.1073/pnas.0806668105

Farr, T., & Kobrick, M. (2000). Shuttle Radar Topography Mission produces a wealth of data. *Eos, Transactions American Geophysical Union*, *81*, 583–585.

Finotello, A., Lentsch, N., & Paola, C. (2019). Experimental delta evolution in tidal environments: Morphologic response to relative sea-level rise and net deposition. *Earth Surface Processes and Landforms*, *44*(10), 2000–2015. https://doi.org/10.1002/esp.4627

Galloway, W. E. (1975). Process framework for describing the morphologic and stratigraphic evolution of deltaic depositional systems. In M. L. Broussard (Ed.), *Deltas, models for exploration* (pp. 86–98). Houston Geological Society. Retrieved from https://archives.datapages.com/data/hgssp/data/022/022001/87_hgs0220087.htm

Ganti, V., Chadwick, A. J., Hassenruck-Gudipati, H. J., Fuller, B. M., & Lamb, M. P. (2016). Experimental river delta size set by multiple floods and backwater hydrodynamics. *Science Advances*, *2*(5), e1501768. https://doi.org/10.1126/sciadv.1501768

Geleynse, N., Storms, J. E. A., Walstra, D.-J. R., Jagers, H. R. A., Wang, Z. B., & Stive, M. J. F. (2011). Controls on river delta formation; insights from numerical modelling. *Earth and Planetary Science Letters*, *302*(1), 217–226. https://doi.org/10.1016/j.epsl.2010.12.013

Geleynse, N., Voller, V. R., Paola, C., & Ganti, V. (2012). Characterization of river delta shorelines. *Geophysical Research Letters*, *39*(17), L17402. https://doi.org/10.1029/2012GL052845

Goodbred, S. L., & Saito, Y. (2012). Tide-dominated deltas. In R. A. Davis Jr. & R. W. Dalrymple (Eds.), *Principles of tidal sedimentology* (pp. 129–149). Springer Netherlands.

Hoitink, A. J. F., Nittrouer, J. A., Passalacqua, P., Shaw, J. B., Langendoen, E. J., Huismans, Y., & van Maren, D. S. (2020). Resilience of river deltas in the anthropocene. *Journal of Geophysical Research: Earth Surface*, *125*(3), e2019JF005201. https://doi.org/10.1029/2019JF005201

Hood, W. G. (2010). Tidal channel meander formation by depositional rather than erosional processes: Examples from the prograding Skagit river delta (Washington, USA). *Earth Surface Processes and Landforms*, *35*(3), 319–330. https://doi.org/10.1002/esp.1920

Hoyal, D. C. J. D., & Sheets, B. A. (2009). Morphodynamic evolution of experimental cohesive deltas. *Journal of Geophysical Research*, *114*(F2), F02009. https://doi.org/10.1029/2007JF000882
Jerolmack, D. J., & Swenson, J. B. (2007). Scaling relationships and evolution of distributary networks on wave-influenced deltas. *Geophysical Research Letters*, *34*(23), L23402. https://doi.org/10.1029/2007GL031823
Kwang, J. S., & Parker, G. (2019). Extreme memory of initial conditions in numerical landscape evolution models. *Geophysical Research Letters*, *46*(12), 6563–6573. https://doi.org/10.1029/2019GL083305
Lauzon, R., & Murray, A. B. (2018). Comparing the cohesive effects of mud and vegetation on delta evolution. *Geophysical Research Letters*, *45*(19), 10437–10445. https://doi.org/10.1029/2018GL079405
Lauzon, R., Piliouras, A., & Rowland, J. C. (2019). Ice and permafrost effects on delta morphology and channel dynamics. *Geophysical Research Letters*, *46*(12), 6574–6582. https://doi.org/10.1029/2019GL082792
Leonardi, N., Canestrelli, A., Sun, T., & Fagherazzi, S. (2013). Effect of tides on mouth bar morphology and hydrodynamics. *Journal of Geophysical Research: Oceans*, *118*(9), 4169–4183. https://doi.org/10.1002/jgrc.20302
Lesser, G. R., Roelvink, J. A., van Kester, J. A. T. M., & Stelling, G. S. (2004). Development and validation of a three-dimensional morphological model. *Coastal Engineering*, *51*(8–9), 883–915.
Liang, M., Voller, V. R., & Paola, C. (2015). A reduced-complexity model for river delta formation – Part 1: Modeling deltas with channel dynamics. *Earth Surface Dynamics*, *3*(1), 67–86. https://doi.org/10.5194/esurf-3-67-2015
Maselli, V., & Trincardi, F. (2013). Man made deltas. *Scientific Reports*, *3*(1), 1926. https://doi.org/10.1038/srep01926
Mikhailova, M. (2003). Transformation of the Ebro River Delta under the impact of intense human-induced reduction of sediment runoff. *Water Resources*, *30*(30), 370–378. https://doi.org/10.1023/a:1024963911893
Nardin, W., & Fagherazzi, S. (2012). The effect of wind waves on the development of river mouth bars. *Geophysical Research Letters*, *39*(12), L12607. https://doi.org/10.1029/2012GL051788
Nardin, W., Edmonds, D. A., & Fagherazzi, S. (2016). Influence of vegetation on spatial patterns of sediment deposition in deltaic islands during flood. *Advances in Water Resources*, *93*, 236–248. https://doi.org/10.1016/j.advwatres.2016.01.001
Nicholls, R. J., Lincke, D., Hinkel, J., Brown, S., Vafeidis, A. T., Meyssignac, B., et al. (2021). A global analysis of subsidence, relative sea-level change and coastal flood exposure. *Nature Climate Change*, *11*(4), 338–342. https://doi.org/10.1038/s41558-021-00993-z
Nienhuis, J. H., Ashton, A. D., & Giosan, L. (2015). What makes a delta wave-dominated? *Geology*, *43*(6), 511–514. https://doi.org/10.1130/G36518.1
Nienhuis, J. H., Ashton, A. D., Edmonds, D. A., Hoitink, A. J. F., Kettner, A. J., Rowland, J. C., & Törnqvist, T. E. (2020). Global-scale human impact on delta morphology has led to net land area gain. *Nature*, *577*(7791), 514–518. https://doi.org/10.1038/s41586-019-1905-9
Nienhuis, J. H., Ashton, A. D., Roos, P. C., Hulscher, S. J. M. H., & Giosan, L. (2013). Wave reworking of abandoned deltas. *Geophysical Research Letters*, *40*(22), 5899–5903. https://doi.org/10.1002/2013GL058231
Nienhuis, J. H., Hoitink, A. J. F., & Törnqvist, T. E. (2018). Future change to tide-influenced deltas. *Geophysical Research Letters*, *45*(8), 3499–3507. https://doi.org/10.1029/2018GL077638
Passalacqua, P., Lanzoni, S., Paola, C., & Rinaldo, A. (2013). Geomorphic signatures of deltaic processes and vegetation: The Ganges-Brahmaputra-Jamuna case study. *Journal of Geophysical Research: Earth Surface*, *118*(3), 1838–1849. https://doi.org/10.1002/jgrf.20128
Pekel, J.-F., Cottam, A., Gorelick, N., & Belward, A. S. (2016). High-resolution mapping of global surface water and its long-term changes. *Nature*, *540*(7633), 418–422. https://doi.org/10.1038/nature20584
Rossi, V. M., Kim, W., Leva López, J., Edmonds, D., Geleynse, N., Olariu, C., et al. (2016). Impact of tidal currents on delta-channel deepening, stratigraphic architecture, and sediment bypass beyond the shoreline. *Geology*, *44*(11), 927–930. https://doi.org/10.1130/G38334.1
Seybold, H., Andrade, J. S., & Herrmann, H. J. (2007). Modeling river delta formation. *Proceedings of the National Academy of Sciences*, *104*(43), 16804–16809. https://doi.org/10.1073/pnas.0705265104
Shaw, J. B., Wolinsky, M. A., Paola, C., & Voller, V. R. (2008). An image-based method for shoreline mapping on complex coasts. *Geophysical Research Letters*, *35*(12), L12405. https://doi.org/10.1029/2008GL033963
Shirzaei, M., Freymueller, J., Törnqvist, T. E., Galloway, D. L., Dura, T., & Minderhoud, P. S. J. (2020). Measuring, modelling and projecting coastal land subsidence. *Nature Reviews Earth & Environment*, *2*(1), 40–58. https://doi.org/10.1038/s43017-020-00115-x
Syvitski, J. P. M., & Saito, Y. (2007). Morphodynamics of deltas under the influence of humans. *Global and Planetary Change*, *57*(3), 261–282. https://doi.org/10.1016/j.gloplacha.2006.12.001
Tejedor, A., Longjas, A., Zaliapin, I., & Foufoula-Georgiou, E. (2015). Delta channel networks: 2. Metrics of topologic and dynamic complexity for delta comparison, physical inference, and vulnerability assessment. *Water Resources Research*, *51*(6), 4019–4045. https://doi.org/10.1002/2014WR016604
Tessler, Z. D., Vorosmarty, C. J., Grossberg, M., Gladkova, I., Aizenman, H., Syvitski, J., & Foufoula-Georgiou, E. (2015). Profiling risk and sustainability in coastal deltas of the world. *Science*, *349*(6248), 638–643. https://doi.org/10.1126/science.aab3574
Wright, L. D., & Coleman, J. M. (1973). Variations in morphology of major river deltas as functions of ocean wave and river discharge Regimes1. *AAPG Bulletin*, *57*(2), 370–398. https://doi.org/10.1306/819A4274-16C5-11D7-8645000102C1865D

References From the Supporting Information

Baar, A. W., Boechat Albernaz, M., Van Dijk, W. M., & Kleinhans, M. G. (2019). Critical dependence of morphodynamic models of fluvial and tidal systems on empirical downslope sediment transport. *Nature Communications*, *10*(1), 4903. https://doi.org/10.1038/s41467-019-12753-x
Dean, R. G. (1991). Equilibrium beach profiles: Characteristics and applications. *Journal of Coastal Research*, *7*(1), 53–84.
Soulsby, R. L. (1997). Dynamics of marine sands: A manual for practical applications. *Oceanographic Literature Review*, *44*(9), 947.